

# The Karlqvist approximation revisited

C. Tannous

Laboratoire de Magnétisme de Bretagne - CNRS FRE 3117  
UBO, 6, Avenue le Gorgeu C.S.93837 - 29238 Brest Cedex 3 - FRANCE

(Dated: April 4, 2022)

The Karlqvist approximation signaling the historical beginning of magnetic recording head theory is reviewed and compared to various approaches progressing from Green, Fourier, Conformal mapping that obeys the Sommerfeld edge condition at angular points and leads to exact results.

PACS numbers: 85.70.Kh, 85.70.Li, 75.50.Ss

## I. INTRODUCTION

Karlqvist seminal historical paper<sup>1</sup> is an important landmark and the first building block of magnetic recording theory. Despite all ensuing developments in recording theory it is still used as a standard reference with respect to any model aiming at the description of recording or replay head fields.

Karlqvist work is based on magnetostatics and Green's function theory of partial differential equations since the basic description of head field physics is based on Laplace or Poisson equations the magnetostatic potential must satisfy under certain conditions.

Magnetic playback theory deals with time dependence since tapes and hard disk platters move with respect to head in contrast with our work that deals with static head description.

We concentrate on the description of magnetostatic interactions in 3D simplifying them to 2D in order to fully understand the Karlqvist approximation and its many aspects that lie at the roots of recording theory.

This work can be taught as an application chapter in a general Electromagnetism course at the Graduate level or in an undergraduate class of Partial Differential Equations since physicists might be interested in applying some mathematical methods to solve Laplace and Poisson equations or understanding issues surrounding the development of magnetic recording advances in hard disks and storage media.

Karlqvist approximation is based on a simplified description of the recording head physics (see fig. 1 and fig. 2) to 2D such that it consists of two semi-infinite poles made from a very soft material possessing an infinite permeability. The poles are separated by a gap region and face a semi-infinite plane devoid of any magnetic charges.

In addition a number of simplifying assumptions are made in order to obtain a fully analytic solution to the field created by the poles, such as:

1. Uniform magnetization above poles leading to a zero volume source density.
2. Spatially linear surface source density in the gap.
3. Uniform field  $H_g$  in the gap all the way up to  $y = 0$ .

In reality, it can be uniform only in the case  $y \ll 0$  far from the  $\partial\Omega$  boundary.

4. Ignorance of Sommerfeld radiation condition<sup>2</sup> near angular boundaries such as regions around points  $x = \pm a, y = 0$ .

In this work we review briefly how magnetostatic theory is used for the description of fields created by the head and its interaction with recording media. It is organised as follows. Section 2 describes Green's function theory in 3D and its application to 2D with the Karlqvist approximation delivering the potential and field created by the recording head in the plane on the basis of a simplified Boundary Value Problem (BVP) described above. In section 3, Karlqvist solution is revised and compared to exact Fourier methods meant to solve the exact BVP. In section 4 we use conformal mapping methods to retrieve the solution for a more realistic head accounting for edge condition at angular points and leading to exact results. Finally section 5 bears conclusions and perspectives of the work.

## II. GREEN'S FUNCTION APPROACH

In the 3D magnetostatic approximation, Maxwell equations for fields  $\mathbf{E}$  and  $\mathbf{H}$  reduce to:

$$\nabla \times \mathbf{E} = 0, \quad \nabla \times \mathbf{H} = 0 \quad (1)$$

In the absence of magnetization and poles ( $\nabla \cdot \mathbf{B} = 0$ ) we infer existence of a magnetic scalar potential  $\phi(\mathbf{r})$  at any point  $\mathbf{r}$  leading to  $\mathbf{H}$  definition and Laplace equation:

$$\mathbf{H} = -\nabla\phi(\mathbf{r}), \quad \Delta\phi(\mathbf{r}) = 0 \quad (2)$$

In presence of a magnetization field  $\mathbf{M}(\mathbf{r})$ , the lowest approximation for the "far-field" potential  $\phi(\mathbf{r})$  in a multipole expansion is dipolar leading to a volume source  $\nabla \cdot \mathbf{M}$  and a surface density source  $\mathbf{n} \cdot \mathbf{M}$  where  $\mathbf{n}$  is the outward normal to the finite surface sample embodying  $\mathbf{M}(\mathbf{r})$ .

The potential  $\phi(\mathbf{r})$  can be obtained, from volume source density  $\rho(\mathbf{r}) = -\nabla \cdot \mathbf{M}(\mathbf{r})$  and surface source

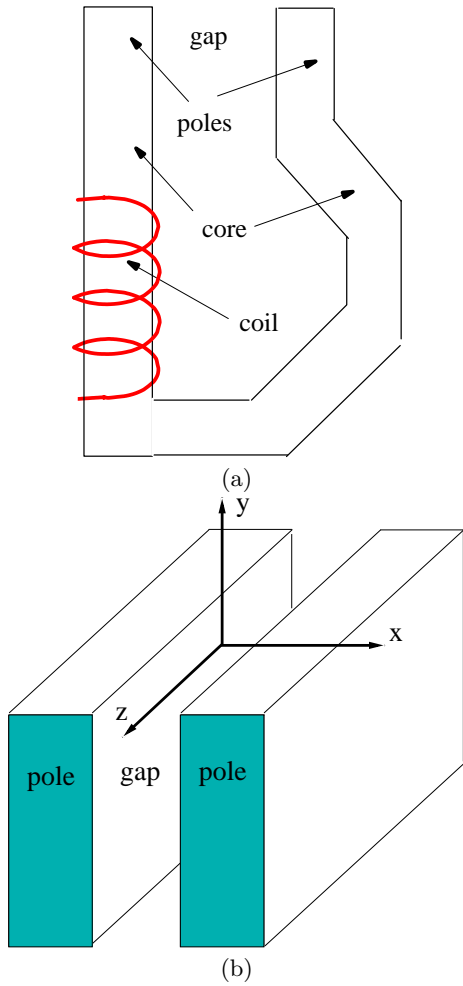


FIG. 1: (a) General structure of a magnetic recording head. Pole and core are generally made from very soft material possessing a very large permeability  $\mu$ . They are excited by a coil that will create a magnetic field in the gap and around the pole surfaces. (b) 3D perspective view of a simplified magnetic recording head tip.

density  $\sigma(\mathbf{r}) = \mathbf{n} \cdot \mathbf{M}(\mathbf{r})$  as (considering free-space permeability  $\mu_0 = 1$ ):

$$\phi(\mathbf{r}) = \frac{1}{4\pi} \int_V \frac{\rho(\mathbf{r}') dV'}{|\mathbf{r} - \mathbf{r}'|} + \frac{1}{4\pi} \oint_{\partial V} \frac{\sigma(\mathbf{r}') dS'}{|\mathbf{r} - \mathbf{r}'|} \quad (3)$$

This result can in fact be reinterpreted as a BVP with a Poisson equation subjected to presence of volume source and surface sources:

$$\Delta\phi(\mathbf{r}) = \nabla \cdot \mathbf{M}, \quad \text{in } V, \quad \phi(\mathbf{r}) = \mathbf{n} \cdot \mathbf{M} \quad \text{on } \partial V \quad (4)$$

It is interesting to note that the surface density is equivalent to a surface potential  $\phi_S(\mathbf{r}) = \mathbf{n} \cdot \mathbf{M}(\mathbf{r})$ .

The BVP eq. 4 can be solved with Green second identity:

$$\int_V [\phi(\mathbf{r}) \Delta G - G \Delta \phi(\mathbf{r})] dV = \oint_{\partial V} [\phi(\mathbf{r}) \nabla G - G \nabla \phi(\mathbf{r})] \cdot \mathbf{n} dS \quad (5)$$

derived from coupling Laplace equation and the definition of the Green's function solution of:

$$\Delta G(\mathbf{r}, \mathbf{r}') = \delta(\mathbf{r} - \mathbf{r}') \quad (6)$$

where  $\delta(\mathbf{r})$  is Dirac delta function.

The radial Green's function expression is obtained by solving the 3D Laplacian in spherical coordinates:

$$\frac{1}{r^2} \frac{\partial}{\partial r} \left( r^2 \frac{\partial G}{\partial r} \right) = 0 \quad \text{for } r > 0 \quad (7)$$

Thus the full Green function  $G(\mathbf{r}, \mathbf{r}') = -\frac{1}{4\pi} \frac{1}{|\mathbf{r} - \mathbf{r}'|}$  is obtained (the angular factor  $4\pi$  originates from solid angle subtending all 3D space) and exploited in expressing the potential as:

$$\phi(\mathbf{r}) = \int_V G(\mathbf{r}, \mathbf{r}') \rho(\mathbf{r}') dV' + \oint_{\partial V} \nabla' G(\mathbf{r}, \mathbf{r}') \cdot \mathbf{n}' \phi_S(\mathbf{r}') dS' \quad (8)$$

Using eq. 6, eq. 4 and the condition  $\nabla \phi(\mathbf{r}) = 0$  on  $\partial V$  we retrieve the general solution for the potential eq. 3.

### A. Karlqvist 2D magnetostatic solution

Karlqvist approximation is based on approximating the magnetic recording head as consisting of the tips only (see fig.1) with the assumption the poles are large and thick and made with an infinitely soft material (permeability  $\mu \approx \infty$ ).

A flat 2D model for the recording head displayed in fig. 2 can be made since poles are considered as infinitely large (along  $x$  direction as in fig. 1) and thick (along  $z$  direction, see fig. 1) separated by the gap region.

With this assumption, one cannot use the potential result previously given in eq. 3 since this is valid strictly in the 3D case.

Thus we move to a fully 2D approach to solve the BVP posed by the magnetic head stated mathematically as:

$$\Delta\phi(\mathbf{r}) = 0 \quad \text{in } \Omega, \quad \phi(\mathbf{r}) = \phi_S(\mathbf{r}) \quad \text{on } \partial\Omega \quad (\text{BVP1}) \quad (9)$$

This means the magnetization field is uniform yielding zero volume source, however we have a non-zero surface potential  $\phi_S(\mathbf{r})$  on  $\partial\Omega$ .

The Green's function of the 2D Laplace equation is  $G(\mathbf{r}, \mathbf{r}') = \frac{1}{2\pi} \ln |\mathbf{r} - \mathbf{r}'|$  obtained by solving the 2D Laplace equation in polar coordinates for the radial part (as in the 3D case,  $2\pi$  corresponds to angle subtending the entire plane):

$$\frac{\partial^2 G}{\partial r^2} + \frac{1}{r} \frac{\partial G}{\partial r} = 0 \text{ for } r > 0 \quad (10)$$

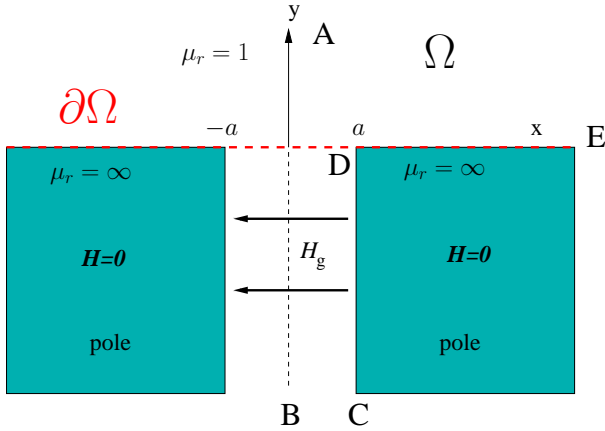


FIG. 2: (Color on-line) 2D approximation of a magnetic recording head. BVP1 eq. 9 is defined by domain  $\Omega$  ( $y > 0$ ) bounded by  $\partial\Omega$  (in dashed red), the entire  $x$  axis. The poles are made from very soft material,  $H = 0$  for any point on  $\partial\Omega$  and inside poles since  $H_g$  is finite in the gap region. Note vertices  $x = \pm a, y = 0$  that should be subject to Sommerfeld radiation condition.

As in the 3D case, the solution to the BVP is obtained from Green second identity over the domains  $\Omega$  and  $\partial\Omega$  corresponding to the previous 3D volume and surface  $V$  and  $\partial V$  respectively using an adequate 2D Green function.

The 2D Green function  $G(\mathbf{r}, \mathbf{r}') = \frac{1}{2\pi} \ln |\mathbf{r} - \mathbf{r}'|$  is for the entire plane whereas in our case, the domain  $\Omega$  is limited to the upper half-plane, thus the Green function should be  $G(\mathbf{r}, \mathbf{r}') = \frac{1}{2\pi} \ln |\mathbf{r} - \mathbf{r}'| - \frac{1}{2\pi} \ln |\mathbf{r} - \tilde{\mathbf{r}}'|$  using the method of images<sup>2</sup>.  $\tilde{\mathbf{r}}' = (x', -y')$  is the image of  $\mathbf{r}' = (x', y')$  in the lower half-plane.

The explicit form of the Green function in the upper half-plane becomes:

$$\begin{aligned} G(\mathbf{r}, \mathbf{r}') &= \frac{1}{2\pi} \ln \left[ \frac{\sqrt{(x-x')^2 + (y-y')^2}}{\sqrt{(x-x')^2 + (y+y')^2}} \right] \\ &= \frac{1}{4\pi} \ln \left[ \frac{(x-x')^2 + (y-y')^2}{(x-x')^2 + (y+y')^2} \right] \end{aligned} \quad (11)$$

Using eq. 6, eq. 9 and  $\nabla\phi(\mathbf{r}) = 0$  on  $\partial\Omega$ :

$$\phi(\mathbf{r}) = \int_{\partial\Omega} \phi_S(\mathbf{r}') \nabla' G(\mathbf{r}, \mathbf{r}') \cdot \mathbf{n}' dS' \quad (12)$$

The quantity  $\nabla' G \cdot \mathbf{n}'$  over the boundary  $\partial\Omega$  is obtained with the outward normal  $\mathbf{n}' = (0, -1)$  as:

$$\nabla' G \cdot \mathbf{n}' = - \left. \frac{\partial G(\mathbf{r}, \mathbf{r}')}{\partial y'} \right|_{y'=0} = \frac{y}{\pi} \frac{1}{[(x-x')^2 + y^2]} \quad (13)$$

yielding:

$$\phi(\mathbf{r}) = \phi(x, y) = \frac{y}{\pi} \int_{-\infty}^{+\infty} \frac{\phi_S(x') dx'}{(x-x')^2 + y^2} \quad (14)$$

The above result called the Poisson integral for the half-plane may be derived from the fact an analytic function can be obtained at any point from the values it takes over a boundary (see for instance Ablowitz *et al.*<sup>3</sup>). It can be viewed as a convolution between the source function  $\phi_S(\mathbf{r})$  and the Green function. The result is retrieved with Fourier analysis in the next section.

Along the boundary  $\partial\Omega$  the source potential function  $\phi_S(x)$  produces the field  $H_g$  in the gap interval  $[-a, +a]$  thus  $H_g = -\frac{d\phi_S}{dx}$  using the definition eq. (2). Outside  $[-a, +a]$  interval, the potential is constant and the field is zero.

In fact the field is created by a current injected in the coil (see fig. 1), as given by Ampère law:  $NI = H_g$  with  $I$  the current and  $N$  the number of coil turns.

The resulting source potential over  $\partial\Omega$  is given by:

$$\phi_S(x) = \begin{cases} -V_0 & x < -a, \\ H_g x & -a < x < a, \\ V_0 & x > a \end{cases} \quad (15)$$

Since  $\phi_S(x)$  is a continuous function we infer that  $V_0 = H_g a = NIa$ .

Over the region  $\Omega$ , the evaluation of the potential  $\phi(x, y)$  requires integration of eq. 12 to get:

$$\phi(x, y) = \frac{H_g}{\pi} \left[ (x+a) \tan^{-1} \left( \frac{x+a}{y} \right) - (x-a) \tan^{-1} \left( \frac{x-a}{y} \right) - \frac{y}{2} \ln \frac{(x+a)^2 + y^2}{(x-a)^2 + y^2} \right] \quad (16)$$

The field components  $H_x(x, y), H_y(x, y)$  over  $\Omega$  ob-

tained from definition (2) are drawn versus  $x/a$  for a

fixed value of  $y/a$  in fig. 3.

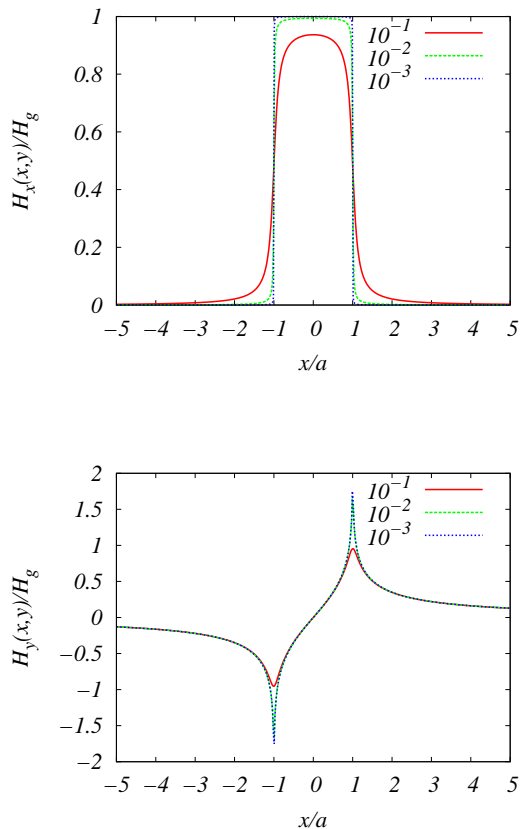


FIG. 3: Variation of the fields  $H_x(x,y), H_y(x,y)$  according to the Karlqvist approximation with  $x$  for fixed  $y/a = 10^{-1}, 10^{-2}, 10^{-3}$ . The edge effect is not visible in  $H_x(x,y)$  whereas it is weaker than reality for  $H_y(x,y)$  (see Conformal Mapping section).

### B. Fourier Transform solution

We retrieve the Green function solution of the Boundary-value problem eq. 9 by introducing the Fourier transform:

$$\Phi(k, y) = \mathcal{F}[\phi(x, y)] = \frac{1}{2\pi} \int_{-\infty}^{+\infty} \phi(x, y) e^{ikx} dx \quad (17)$$

Laplace equation is transformed into:

$$\frac{\partial^2 \Phi(k, y)}{\partial y^2} - k^2 \Phi(k, y) = 0 \text{ for } y > 0 \quad (18)$$

The solution  $\Phi(k, y)$  being a superposition of  $e^{|k|y}$  and  $e^{-|k|y}$ , the acceptable function for  $y > 0$  is  $e^{-|k|y}$  thus  $\Phi(k, y) = \Phi(k, 0)e^{-|k|y}$ . The solution  $\phi(x, y)$  being the inverse Fourier Transform of  $\Phi(k, y)$  and since the latter is the product of two Fourier Transforms  $\Phi(k, 0)$  and  $e^{-|k|y}$ , then by the convolution theorem,  $\phi(x, y)$  is the convolution of the inverse Fourier Transforms of  $\Phi(k, 0)$  and  $e^{-|k|y}$ .

Using the boundary condition  $\phi(x, y = 0) = \phi_S(x)$  from eq. 9 and using Fourier Transform definition 17 results in:

$$\mathcal{F}^{-1}[\Phi(k, 0)] = \mathcal{F}^{-1} \left[ \frac{1}{2\pi} \int_{-\infty}^{+\infty} \phi_S(x) e^{ikx} dx \right] = \phi_S(x) \quad (19)$$

Moreover recall that:

$$\mathcal{F}^{-1}[e^{-|k|y}] = \frac{2y}{x^2 + y^2} \equiv f(x, y) \quad (20)$$

since  $k$  and  $x$  are Fourier Transform pairs.

Applying the convolution theorem to the inverse Fourier Transforms yields the potential as:

$$\begin{aligned} \phi(x, y) &= \frac{1}{2\pi} \int_{-\infty}^{+\infty} \phi_S(x') f(x - x', y) dx' \\ &= \frac{1}{2\pi} \int_{-\infty}^{+\infty} \phi_S(x') \frac{2y}{(x - x')^2 + y^2} dx' \end{aligned} \quad (21)$$

which is exactly the solution eq. 12 found previously with 2D Green's function.

### III. EXACT FOURIER ANALYSIS

Karlqvist solution of BVP1 eq. 9 is now reexamined such that the gap field is no longer imposed. Thus we have another BVP (called BVP2) corresponding to the exact solution given by:

$$\begin{aligned} \Delta \phi(\mathbf{r}) &= 0 \text{ in Regions I and II,} \\ \phi(\mathbf{r}) &= \pm V_0 \text{ on pole surfaces} \end{aligned} \quad (\text{BVP2}) \quad (22)$$

The linear gap potential  $\phi_I(x, y)$  found previously is corrected by adding a Fourier sum<sup>4</sup> with unknown discrete coefficients  $A_n$  in order to satisfy BVP2 eq. 22. The potential  $\phi_{II}(x, y)$  in the upper half-plane is expressed with continuous coefficients  $C(k)$  obtaining:

$$\begin{aligned}\phi_I(x, y) &= H_g x + \sum_{n=0}^{\infty} A_n \sin(n\pi x/a) e^{n\pi y/a} \quad 0 < x < a, \quad y < 0; \\ \phi_{II}(x, y) &= \int_0^{\infty} C(ka) \sin(kx) e^{-ky/a} dk \quad 0 < x < \infty, \quad y > 0\end{aligned}\quad (23)$$

In order to relate both sets of coefficients  $A_n$  and  $C(ka)$ , we match the potential and derivative at  $y = 0$  obtaining:

$$C(ka) = -\frac{I \sin(ka)}{\pi (ka)^2} - \sum_{n=1}^{\infty} (-1)^n 2n A_n \frac{\sin(ka)}{(ka)^2 - (n\pi)^2} \quad (24)$$

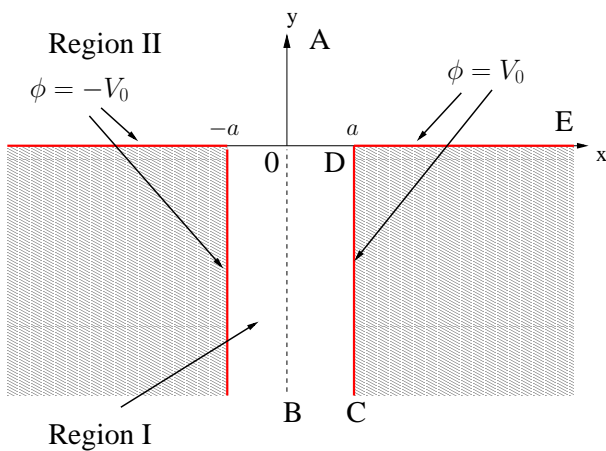


FIG. 4: (Color on-line) Regions I and II where  $\Delta\phi(\mathbf{r}) = 0$  are bounded by red borderlines defining BVP2 eq. 22 with pole surfaces considered as two distinct equipotentials  $\phi = \pm V_0$ .

Eliminating coefficients  $C(ka)$  allows us to derive relations among  $A_m$  coefficients:

$$\frac{A_m}{2} = \frac{2}{\pi} (-1)^{m+1} \left[ \sum_{n=1}^{\infty} (-1)^n n\pi A_n I_{mn} + H_g I_{m0} \right] \quad (25)$$

The coefficients  $I_{nm}$  are given in the Appendix. The above constitute an infinite Algebraic system of linear equations that can be solved after numerical truncation and performing LU decomposition techniques<sup>5</sup> (see Appendix). However it is preferable to use the exact values obtained from the combination of Fourier results and conformal mapping described in the next section since the accuracy of the numerical values of  $A_m$  decreases with the order  $m$  when LU decomposition is performed.

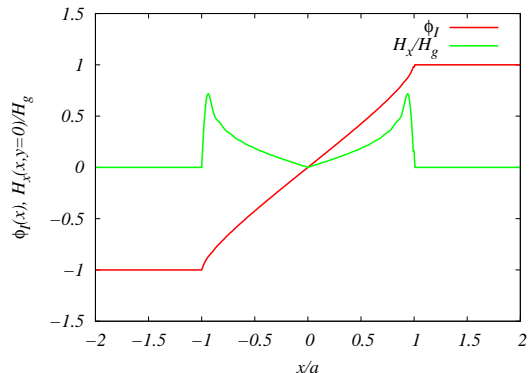


FIG. 5: Fourier reconstructed potential  $\phi_I(x, y = 0)$  and field  $H_x(x, y = 0)$  in the gap. Field oscillations due to Gibbs phenomenon arise from finite sum of Fourier coefficients. They are damped with Sigma Lanczos factors affecting as well the edge effect.

#### IV. CONFORMAL MAPPING

The Schwarz-Christoffel transformation<sup>3</sup> is used to map the semi-infinite pole region of the  $z$ -plane onto the real axis in the complex  $w$  plane (see fig. 2).

A polygon with vertices  $a_i$  located in the  $z$  plane with interior angles  $\alpha_i$  is transformed into a sequence of points  $w_1, w_2, \dots$  along the real axis in the  $w$  plane with (see fig. 6):

$$\frac{dz}{dw} = \gamma (w - w_1)^{(\alpha_1/\pi) - 1} (w - w_2)^{(\alpha_2/\pi) - 1} (w - w_3)^{(\alpha_3/\pi) - 1} \dots \quad (26)$$

The inspection of polygon ABCDE in the  $z$  plane (see fig. 2) maps BCD vertices with corresponding angles:  $\alpha_1 = \frac{\pi}{2}, \alpha_2 = \frac{\pi}{2}, \alpha_3 = \frac{3\pi}{2}$  into B'C'D' with abscissae  $w_1 = w_2 = 0, w_3 = 1$  with Schwarz-Christoffel relation:

$$\frac{dz}{dw} = \gamma \frac{\sqrt{w-1}}{w} \quad (27)$$

where  $\gamma$  is a complex constant to be determined. Integration of eq. 27 yields:

$$z = 2\gamma(\sqrt{w-1} - \tan^{-1} \sqrt{w-1}) + z_0 \quad (28)$$

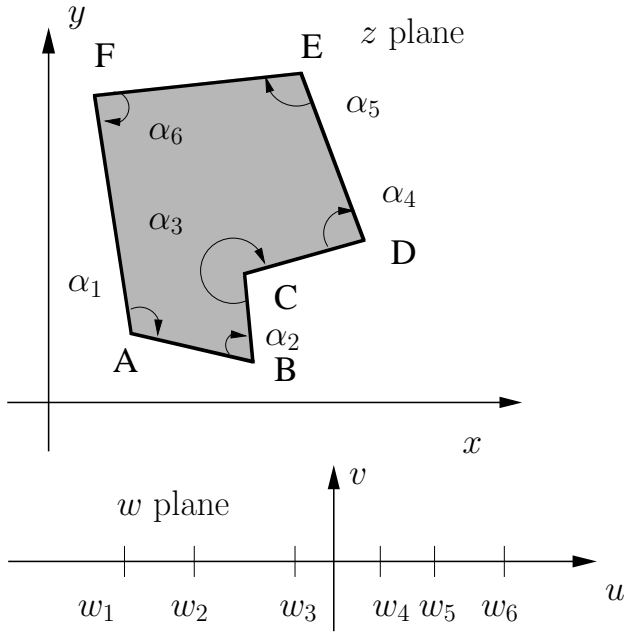


FIG. 6: Schwarz-Christoffel mapping of the polygonal region ABCDEF of the  $z$ -plane onto  $w_1, w_2, \dots, w_6$  on the real axis of the complex  $w$  plane.

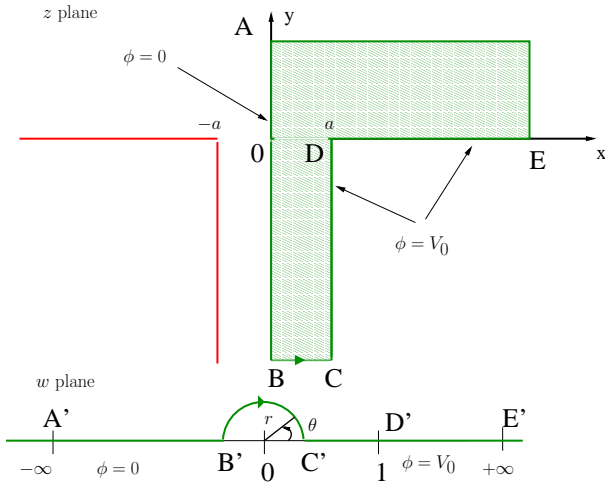


FIG. 7: The polygonal region ABCDE in the  $z$  plane is mapped onto  $A'B'C'D'E'$  along the real axis of the complex  $w$  plane. Line BC is mapped to the line  $B'C'$  deformed into a half-circle with vanishing radius  $r \rightarrow 0$  to allow reveal the angle  $\theta$  as 0 for  $C'$  and  $\pi$  for  $B'$ . The potential  $\phi = 0$  over  $A'B'$  and  $\phi = V_0$  over  $C'D'E'$ .

Using  $\tan^{-1} z = -i \tanh^{-1}(iz)$  and  $\tanh^{-1}(iz) = \frac{1}{2} \ln\left(\frac{1+iz}{1-iz}\right)$  gives:

$$z = 2\gamma \left[ \sqrt{w-1} + \frac{i}{2} \ln \left( \frac{1+i\sqrt{w-1}}{1-i\sqrt{w-1}} \right) \right] + z_0 \quad (29)$$

In order to evaluate the unknowns  $\gamma$  and  $z_0$  we use the map eq. 28 D to  $D'$  thus  $w = 1$  corresponds to  $z = a$  and

we use the Schwarz-Christoffel transformation 27 to get:

$$\int_B^C dz = \int_{B'}^{C'} \gamma \frac{\sqrt{w-1}}{w} dw \quad (30)$$

This contour integral is evaluated with the replacement  $w = re^{i\theta}$  with  $r \rightarrow 0$  such that  $B'$  corresponds to  $\theta = \pi$  and  $C'$  to  $\theta = 0$ :

$$a = \lim_{r \rightarrow 0} \int_{\pi}^0 \gamma \frac{\sqrt{[re^{i\theta}-1]}}{re^{i\theta}} ire^{i\theta} d\theta = \gamma\pi \quad (31)$$

Thus  $\gamma = a/\pi$  and  $z_0 = a$ .

After conformal mapping, we define an analytic complex function<sup>6</sup>  $F(w) = \psi + i\phi = -\frac{V_0}{\pi} \ln w + iV_0$  built with the magnetostatic flux  $\psi$  and the potential  $\phi$  satisfying the boundary conditions in the  $w$  plane, namely:  $\phi = 0$  along  $A'B'$  (since  $\arg(w) = \pi$ ),  $\phi = V_0$  along  $C'D'$  and  $D'E'$  ( $\arg(w) = 0$ ) (see fig. 2).

The magnetic field is obtained from  $F(w)$  after differentiating with the complex operators  $\frac{\partial}{\partial x} = \left(\frac{\partial}{\partial z} + \frac{\partial}{\partial \bar{z}}\right)$  and  $\frac{\partial}{\partial y} = i\left(\frac{\partial}{\partial z} - \frac{\partial}{\partial \bar{z}}\right)$  that transform field expression (2) into a 2D complex form with  $H_x = -\text{Im} \left[ \frac{dF(w)}{dz} \right]$  and  $H_y = -\text{Re} \left[ \frac{dF(w)}{dz} \right]$ .

The fields  $H_x(x, y)$ ,  $H_y(x, y)$  are obtained after relating  $w$  to  $z = x + iy$  using relation 29 and drawn versus  $x/a$  for a fixed value of  $y/a$  in fig. 8.

$H_x(x, y)$  and  $H_y(x, y)$  behave around the edges according to the Sommerfeld radiation condition<sup>2</sup>. We find that  $H_x, H_y \sim y^{-\frac{1}{3}}$  for  $x \approx \pm a$  which is expected from the edge rule stating that the fields near an edge behave as  $\frac{1}{\rho^{1-\nu}}$  with  $\nu = \frac{\pi}{(2\pi-\alpha)}$  where  $\rho$  is the distance to the edge and  $\alpha$  the edge angle. Applied to our case, we have  $y = \rho, \alpha = \frac{\pi}{2}$  yielding  $\nu = \frac{2}{3}$  thus the  $y^{-\frac{1}{3}}$  behaviour confirmed by Matzner *et al.*<sup>7</sup>.

### A. Exact Fourier $A_m$ coefficients

Conformal mapping is now used to extract the exact<sup>8</sup>  $A_n$  coefficients that are used in the Fourier solution eq. 23.

Since the gap solution given by  $A_n$  coefficients that are related to the half-space solution coefficients given by  $C(ka)$ , it might be useful to turn to Fourier transform of the fields obtained from the conformal transformation.

The Fourier transform (cf. definition 17) of the head magnetic field  $\mathcal{F}[H_x(x, y)]$  is related to the potential  $\phi(x, y)$  Fourier transform via  $C(ka)$  such that<sup>8</sup>:

$$\begin{aligned} \mathcal{F}[\phi(x, y)] &= -\frac{i\pi a}{2} C(ka) e^{ky}, \\ \mathcal{F}[H_x(x, y)] &= -\frac{k\pi a}{2} C(ka) e^{ky}. \end{aligned} \quad (32)$$

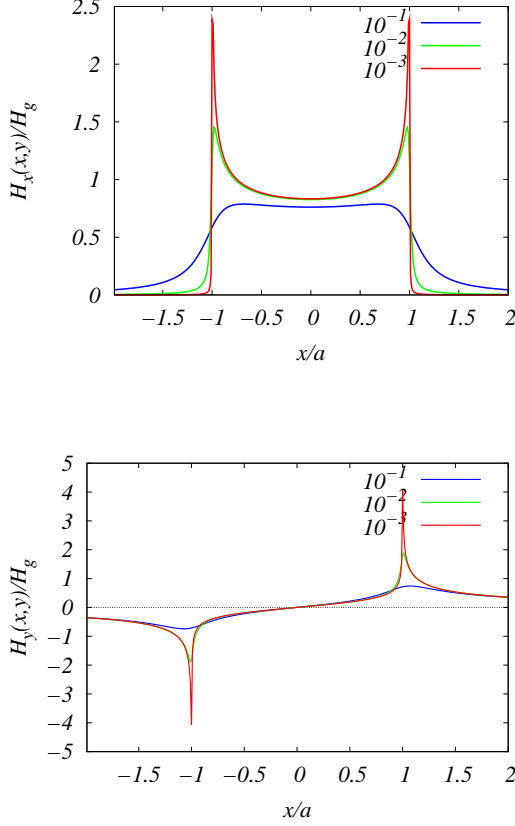


FIG. 8: Variation of the fields  $H_x(x, y)$ ,  $H_y(x, y)$  with  $x/a$  for fixed  $y/a = 10^{-1}, 10^{-2}, 10^{-3}$ . Sommerfeld radiation singularities at  $x = \pm a$  edges are enhanced as  $y/a$  decreases.

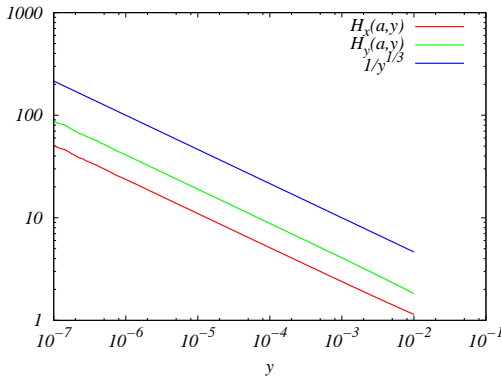


FIG. 9: Scaling with  $y$  of the edge fields  $H_x(a, y)$ ,  $H_y(a, y)$  confirming the radiation condition exponent predicted<sup>2</sup> as  $1/3$ .

Using  $ka = m\pi$  in the  $C(ka)$  expression 24 yields:

$$A_m = \frac{1}{m\pi} \mathcal{F}[H_x(x, y)] e^{m\pi y/a} \quad (33)$$

Taking  $y = 0$  gives  $A_m = \frac{1}{m\pi} \mathcal{F}[H_x(x, 0)]$  and using relation  $\mathcal{F}[H_x(x, 0)] = V_0 S(ka)$  with  $S$  given by Wilton *et al.*<sup>8</sup>:

$$S(m\pi) = \text{Im} \left[ \frac{1}{2\pi} \int_{-\infty}^{+\infty} \frac{s}{s^2 + 1} \left( \frac{s+i}{s-i} \right)^m e^{2mis} ds \right], \quad (34)$$

it suffices to calculate the above integral in order to evaluate the exact  $A_m$  coefficients.

The integral is straightforwardly calculated by complex contour integration<sup>8</sup>. There is a single pole  $s = i$  of order  $m + 1$  in the upper half-plane. Integrating over the real axis and closing the contour by a half-circle in the upper half-plane, we obtain from the  $\frac{1}{(s-i)}$  coefficient of the  $S(m\pi)$  Laurent series the value  $K_m e^{-2m}$  with:

$$K_m = \sum_{n=0}^{m-1} \binom{m-1}{n} \frac{m+n}{(m-n)!} (-)^{m-n} (4m)^{m-n-1} \quad (35)$$

The coefficients  $A_m = \frac{2e^{-2m}}{m\pi} K_m$  are given in the Appendix and compared to Fourier results.

## V. CONCLUSION AND PERSPECTIVES

The Karlqvist approximation pioneered study of magnetic recording and replay heads. It is a very important landmark in the history of recording.

Karlqvist made a very elaborate approach based on a specific BVP (called BVP1) he solved with Green's function techniques that were very popular at the time of his work.

While Karlqvist solution is based on a constant gap field, Fourier methods and conformal mapping methods tackle the Laplace problem directly as a boundary value problem called BVP2 without considering the constant gap field assumption to obtain a more accurate and realistic description of the head field satisfying Sommerfeld edge condition at angular points.

While Green's function is important and yields several fundamental results, it lacks the flexibility and versatility of conformal mapping that allows to derive the scaling law at the edge points as well as evaluate the exact Fourier expansion coefficients.

It is remarkable that it took 40 years<sup>9</sup> to calculate the exact coefficients for a straightforward Laplace problem consisting of two semi-infinite equipotential domains separated by a gap and facing a free half-plane. Using popular software packages, be they symbolic (like Mathematica or Maple) and Finite-Element Method based such as

COMSOL-Multiphysics can approach the problem readily with varying degree of success but miss the physical points raised in this work.

In spite of all developments in magnetic recording theory, Karlqvist approximation remains a major milestone in recording physics and is always used as a standard gauge with respect to any recording theory.

### Appendix A: Evaluation of the exact Fourier Coefficients

The numerical evaluation of the exact  $A_n$  is straightforward but the evaluation of the infinite algebraic system of equations eq. 25 is tricky since it involves non-trivial intermediate operations such as infinite summations, evaluation of the  $I_{mn}, I_{m0}$  integrals... In addition, the presence of minus signs in the system might induce numerical conditioning<sup>5</sup>.

Since the  $A_m$  coefficients satisfy the relations (taking  $H_g = 1$  in eq. 25):

$$\frac{A_m}{2} = \frac{2}{\pi}(-1)^{m+1} \left[ \sum_{n=1}^{\infty} (-1)^n n \pi A_n I_{mn} + I_{m0} \right] \quad (\text{A1})$$

it is possible to write<sup>9</sup> for them a linear system  $M\mathbf{x} = \mathbf{b}$  where the matrix  $M$  elements are given by:

$$M_{mn} = (-1)^{m+n} n \pi I_{mn} + \begin{cases} \frac{\pi}{4} & m = n, \quad m = 1, 2, 3... \\ 0 & m \neq n, \quad n = 1, 2, 3... \end{cases} \quad (\text{A2})$$

the unknowns  $x_m = A_m$  and the RHS terms are given by  $b_m = (-1)^{m+1} I_{m0}, m = 1, 2, 3, \dots$

The  $I_{mn}$  terms are integrals given by:

$$I_{mn} = \int_0^{\infty} \frac{x \sin^2 x}{[x^2 - (m\pi)^2][x^2 - (n\pi)^2]} dx \quad (\text{A3})$$

can be expressed after partial fraction decomposition into simpler integrals of the form:

$$J_m = \int_0^{\infty} \frac{x \sin^2 x}{[x^2 - (m\pi)^2]} dx = \frac{1}{2} \left[ \int_0^{\infty} \frac{x}{[x^2 - (m\pi)^2]} dx - L_m \right] \quad (\text{A4})$$

where:

$$L_m = \int_0^{\infty} \frac{x \cos 2x}{[x^2 - (m\pi)^2]} dx \quad (\text{A5})$$

Integrals  $L_m$  can be evaluated with contour integration<sup>3</sup> or obtained from Gradshteyn-Ryzhik tables<sup>10</sup>. As a result, terms  $I_{mn}, I_{mm}$  and  $I_{m0}$  are expressed analyti-

cally as:

$$\begin{aligned} I_{mn} &= \frac{[\ln(m/n) - Ci(2m\pi) + Ci(2n\pi)]}{2\pi^2(n^2 - m^2)} & n \neq m, \\ I_{mm} &= \frac{Si(2m\pi)}{2m\pi} & n = m, \\ I_{m0} &= -\frac{1}{2m^2\pi^2} [\gamma_E + \ln(2m\pi) - Ci(2m\pi)] & n = 0 \end{aligned}$$

where  $\gamma_E = 0.57721566\dots$  is Euler-Mascheroni<sup>11</sup> constant and  $Ci(x), Si(x)$  are the cosine and sine integrals<sup>11</sup> given respectively by:

$$Ci(x) = -\int_x^{\infty} \frac{\cos(t)}{t} dt, \quad Si(x) = \int_0^x \frac{\sin(t)}{t} dt \quad (\text{A6})$$

In order to solve the system with LU decomposition<sup>5</sup> we truncate it to an  $N \times N$  system with  $N$  taken successively as  $N = 100, 200, \dots, 1000$ . The convergence is monitored by comparing the LU coefficients to the exact coefficients as  $N$  varies. After establishment of convergence, a value of  $N = 1000$  allows us to assess the accuracy in the evaluation of  $A_m$  as  $m$  increases (see Table I).

$n$	Exact	LU decomposition	Wilton <i>et al.</i> <sup>9</sup>
1	$-8.6157113 \times 10^{-2}$	$-8.6155161 \times 10^{-2}$	$-8.6157121 \times 10^{-2}$
2	$2.9150246 \times 10^{-2}$	$2.9149190 \times 10^{-2}$	$2.9150244 \times 10^{-2}$
3	$-1.5254218 \times 10^{-2}$	$-1.5253429 \times 10^{-2}$	$-1.5254219 \times 10^{-2}$
4	$9.5924977 \times 10^{-3}$	$9.5917108 \times 10^{-3}$	$9.5924996 \times 10^{-3}$
5	$-6.6803270 \times 10^{-3}$	$-6.6796015 \times 10^{-3}$	$-6.6803293 \times 10^{-3}$
6	$4.9651614 \times 10^{-3}$	$4.9644802 \times 10^{-3}$	$4.9651619 \times 10^{-3}$
7	$-3.8608240 \times 10^{-3}$	$-3.8602557 \times 10^{-3}$	$-3.8608965 \times 10^{-3}$
8	$3.1035715 \times 10^{-3}$	$3.1029664 \times 10^{-3}$	$3.1035778 \times 10^{-3}$
9	$-2.5590272 \times 10^{-3}$	$-2.5585052 \times 10^{-3}$	$-2.5590907 \times 10^{-3}$
10	$2.1529666 \times 10^{-3}$	$2.1524425 \times 10^{-3}$	$2.1530113 \times 10^{-3}$
11	$-1.8415294 \times 10^{-3}$	$-1.8406087 \times 10^{-3}$	$-1.8411567 \times 10^{-3}$
12	$1.5957345 \times 10^{-3}$	$1.5953275 \times 10^{-3}$	$1.5958599 \times 10^{-3}$
13	$-1.3977018 \times 10^{-3}$	$-1.3985117 \times 10^{-3}$	$-1.3990281 \times 10^{-3}$
14	$1.2364594 \times 10^{-3}$	$1.2378943 \times 10^{-3}$	$1.2383976 \times 10^{-3}$
15	$-1.1009253 \times 10^{-3}$	$-1.1049084 \times 10^{-3}$	$-1.1054002 \times 10^{-3}$
16	$9.9083269 \times 10^{-4}$	$9.9341292 \times 10^{-4}$	$9.9389255 \times 10^{-4}$
17	$-8.9483510 \times 10^{-4}$	$-8.9890108 \times 10^{-4}$	$-8.9937093 \times 10^{-4}$
18	$8.2353526 \times 10^{-4}$	$8.1800920 \times 10^{-4}$	$8.1846816 \times 10^{-4}$
19	$-7.4235769 \times 10^{-4}$	$-7.4817217 \times 10^{-4}$	$-7.4862316 \times 10^{-4}$
20	$7.0718257 \times 10^{-4}$	$6.8741635 \times 10^{-4}$	$6.8785821 \times 10^{-4}$

TABLE I: Exact, LU decomposition and Wilton *et al.* evaluated  $A_n$  coefficients<sup>9</sup>. As  $n$  increases, the discrepancy in the coefficients originates from decrease in accuracy of the LU decomposition.

- 
- <sup>1</sup> O. Karlqvist, "Calculation of the Magnetic Field in The Ferromagnetic Layer of a Magnetic Drum", Trans. Roy. Inst. Techno., Stockholm, No. 86, 3 (1954).
  - <sup>2</sup> J. G. Van Bladel, *Singular Electromagnetic Fields and Sources*, Wiley-IEEE Press, New-York (1996).
  - <sup>3</sup> M. Ablowitz and A. Fokas, *Complex variables: Introduction and Applications*, 2nd edition, p. 287, Cambridge University Press, New-York (2003).
  - <sup>4</sup> G. J. Y. Fan, "A Study of The Playback Process of a Magnetic Ring Head", IBM J. of Res. and Dev. 5, 321 (1961). Fan paper contains many typos that are corrected in: H.L. Huang and H. Y. Deng, "Comparison of Ring Head and SPT Head Write Fields", IEEE Trans. Magn., Vol. 22, 1305 (1986).
  - <sup>5</sup> W. H. Press, W. T. Vetterling, S. A. Teukolsky and B. P. Flannery, *Numerical Recipes in C: The Art of Scientific Computing* Second Edition, Cambridge University Press, New-York (1992).
  - <sup>6</sup> G. A. Bertero, H. N. Bertram and D. M. Barnett, "Fields and Transforms for Thin Film Heads", IEEE Trans. Magn., Vol. 29, 67 (1993).
  - <sup>7</sup> H. Matzner and S. Shtrikman, "Some improved formulas for the Westmijze head", IEEE Trans. Magn., Vol. 33, 820 (1997).
  - <sup>8</sup> D. T. Wilton, B. K. Middleton and M. Aziz, "Exact Harmonic Coefficients for a Magnetic Ring Head", IEEE Trans. Magn., Vol. 35, 2043 (1999).
  - <sup>9</sup> D. T. Wilton, "Comparison of Ring and Pole Head magnetic fields", IEEE Trans. Magn., Vol. 26, 1229 (1990).
  - <sup>10</sup> I. S. Gradshteyn, I. M. Ryzhik, *Tables of Integrals, Series and Products*, 7th edition, Academic Press, New-York (2007) p.424, 3.723(11)
  - <sup>11</sup> M. Abramowitz and I.S Stegun, *Handbook of Mathematical Tables*, Dover, New-York (1960).